



Electrochemical sensors based on platinum-coated MOF-derived nickel-/N-doped carbon nanotubes (Pt/Ni/NCNTs) for sensitive nitrite detection

Shuyue Wang¹ · Haoyong Yin¹ · Kaige Qu¹ · Ling Wang² · Jianying Gong¹ · Shumin Zhao¹ · Shengji Wu³

Received: 14 January 2023 / Accepted: 30 March 2023 / Published online: 11 April 2023
© The Author(s), under exclusive licence to The Japan Society for Analytical Chemistry 2023

Abstract

As excess nitrite has a serious threat to the human health and environment, constructing novel electrochemical sensors for sensitive nitrite detection is of great importance. In this report, platinum nanoparticles were deposited on nickel-/N-doped carbon nanotubes, which were obtained through a self-catalytically grown process with Ni-MOF as precursors. The as-prepared Pt/Ni/NCNTs were applied as amperometric sensors and presented superior sensing properties for nitrite detection. Benefiting from the synergy of Pt and Ni/NCNTs, Pt/Ni/NCNTs displayed much wider detection ranges (0.5–40 mM and 40–110 mM) for nitrite sensing. The sensitivity is $276.92 \mu\text{A mM}^{-1} \text{cm}^{-2}$ and $224.39 \mu\text{A mM}^{-1} \text{cm}^{-2}$, respectively. The detection limit is $0.17 \mu\text{M}$. The Pt/Ni/NCNTs sensors also showed good feasibility for nitrite sensing in real samples (milk and peach juice) analysis. The active Pt/Ni/NCNTs composites and facile fabrication technique may provide useful strategies to develop other sensitive nitrite sensors.

Keywords Platinum · Nickel · Carbon nanotubes · Nitrite · Electrochemical sensors

Introduction

With the wide application of nitrite in various fields, such as fertilizer industries and food preservation, its impact on human health and environmental safety has attracted more and more attention. The maximum allowable content of nitrite is ruled by WHO to be 3 mg/L (65.2 μM) in drinking water, as it is a typical carcinogen that threatens human health. In addition, nitrite can also lead to the blue baby syndrome when excessive nitrite ions in blood react with hemoglobin, which may reduce the oxygen transport capability of blood [1–3]. Consequently, the accurate and rapid

nitrite detection is extremely vital to both human health and environmental security.

Nowadays, tremendous efforts have been put to develop highly effective protocol for nitrite detection. Various techniques, such as chemiluminescence [4], fluorescence [5], spectroscopy [6], chromatography [7], and electrochemical methods [1], all displayed their unique advantages in nitrite sensing. Among them, electrochemical methods are receiving more and more attention owing to their advantages of fast response, easy operation, high sensitivity, and low cost. Generally, the sensing properties of nitrite sensors relay highly on the electro-catalytic reaction (including the oxidation and reduction of nitrite) on the electrode surface. As the oxidation route can prevent the interference from impurities, such as nitrate ion and molecular oxygen, electrochemical oxidation sensors are preferred in nitrite detection. Thus, the electro-catalysts are critical to the sensing performance as their catalytic activity greatly determines the current signal of nitrite oxidation. Up till now, considerable transition metals and their oxides have aroused great attention in nitrite sensing on account of their superior catalytic activity. For instance, NiCo_2O_4 nano-tapes were obtained through microwave-assisted methods and displayed electro-catalytically activities toward the oxidation of nitrite [8].

✉ Haoyong Yin
yhy@hdu.edu.cn

✉ Shengji Wu
wushengji26@hdu.edu.cn

¹ Wenzhou Institute of Hangzhou Dianzi University,
Wenzhou 325038, China

² Department of Chemistry, Zhejiang Sci-Tech University,
Hangzhou 310018, China

³ College of Engineering, Huzhou University, Huzhou 313000,
China

MoO₃/Co₃O₄ hetero-structure presented preferable sensing performance for detecting nitrite in sausages and water [9]. NiFe-layered double hydroxide also showed great prospect in highly sensitive nitrite detection [10]. Especially, nickel-based materials (such as Nickel Phosphide [11], Nickel Oxide [12], and Nickel Hydroxide [13]) attracted more attention in nitrite sensing owing to their low cost, good catalytic activity, and remarkable chemical stability. However, the sensing properties of these transition metals including nickels are still unsatisfied mainly owing to their intrinsic poor conductivity.

As typical carbon materials, carbon nanotubes (CNTs) have been intensively studied as host materials for transition metals or their compounds to improve their electrochemical activities due to their high conductivity and large surface specific area. For instance, the α -Fe₂O₃/CNTs hybrid modified electrode displayed highly improved activity for nitrite oxidation [14]. Co₃O₄-rGO/CNTs [15] and Cu₂O/CNTs composites [16] all demonstrated superior properties for sensitive and selective detection of nitrite. However, the application of CNTs composite materials still faces severe challenges. Especially, the combination of CNTs and catalyst particles is not strong enough, which will greatly affect the charge transfer efficiency and stability of materials. Previous research suggested that self-catalytically grown metals/NCNTs composites (such as Co/NCNTs [17], NiFe Alloy/NCNTs [18], and NiCo/NCNTs [19]) can greatly enhance the combination of NCNTs and metal particles and result in improved charge and mass transfer efficiency. Another challenge for transition metal/CNTs on nitrite sensing is that the activity is still unsatisfied for practical application and the operating voltage is also relatively high for nitrite oxidation. Combining Pt with electrode materials may both improve their nitrite sensing performance and reduce the operating voltage due to its good conductivity and superior catalytic activity. In addition, NCNTs may also prevent the aggregation of Pt nanoparticles as the doped nitrogen may provide nucleation and growth sites to anchor Pt nanoparticles.

Herein, we present a new electrochemical sensing material of Pt/Ni/NCNTs for nitrite detection. The Ni/NCNTs were first obtained through a self-catalyzed growth process with nickel-based metal-organic frameworks (Ni-MOF) as carbon, nitrogen, and nickel source. Pt nanoparticles were then deposited on Ni/NCNTs with a microwave assistant synthesis method. Metal-organic frameworks (MOFs) are a class of ordered porous crystalline materials consisted of metal ions and organic linkers, which can be used as self-sacrificial templates to construct metal@carbon hybrids for electrode modification with the structure and morphology of parent MOFs always maintained. Therefore, the self-catalyzed growth of Ni/NCNTs from Ni-MOF can ensure the tight contact of NCNTs and Ni greatly, lowering their interface contact resistance. Moreover, the nitrogen doping

in NCNTs may not only modulate the electric structures of CNTs but also benefit to the dispersion of Pt nanoparticles on NCNTs. The integration of Pt and Ni with NCNTs can afford more active sites. In addition, the operating voltage of nitrite oxidation has also been reduced in this system.

Experimental section

Preparation of Ni/NCNTs

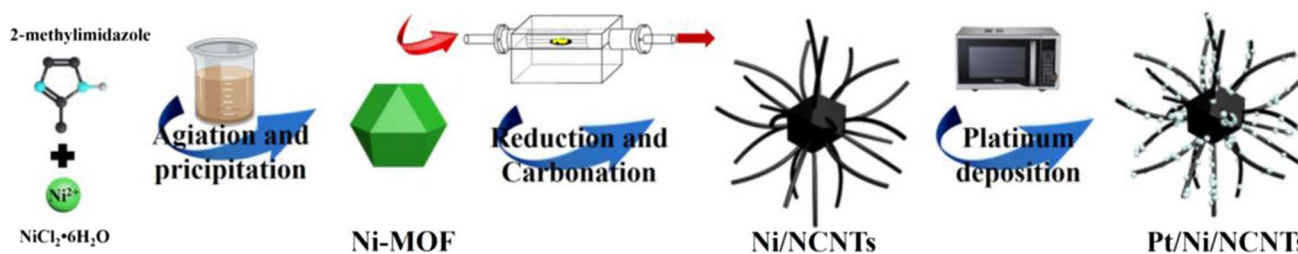
Ni/NCNTs were obtained through the thermal decomposition method with Ni-MOFs as precursors. Typically, 1.188 g NiCl₂•6H₂O was first dissolved into 100 ml methanol to form solution A. Solution B was obtained by dissolving 3.284 g 2-methylimidazole into another 100 ml methanol. Then, solution B was slowly added into solution A under continuous stirring for 24 h at room temperature. The mixture was then centrifuged at 4000 r/min to separate the product and washed several times with deionized water and dried overnight at 60 °C. Finally, the samples were calcined at 900 °C for 2 h under N₂ atmosphere with a heating rate of 2 °C/min and a cooling rate of 5 °C/min to obtain Ni/NCNTs composites.

Preparation of Pt/Ni/NCNTs

In typical, 0.042 g Ni/NCNTs composites were first dispersed into 20 ml ethylene glycol and sonicated for 10 min. Then, 715 μ L of 1 M H₂PtCl₆ solution was added into the above mixed solution and continued to sonicate for another 10 min. The suspension was subsequently transferred into a microwave oven and treated with microwave power of 800 W three times for 30 s, 30 s, and 15 s, respectively. Finally, the Pt/Ni/NCNTs composite was obtained after washing it with deionized water and drying it at 60 °C.

Measurements and characterization

Electrochemical measurements were performed on CHI630D workstation (Shanghai Chenhua Instrument Co. China). Supporting electrolyte used in Cyclic voltammetry (CV), amperometric (I-T), and differential pulse voltammetry (DPV) measurements is 0.1 M phosphate solution (PBS), which was bubbled with N₂ for about 15 min before the test to remove dissolved oxygen. The glassy carbon electrode (GCE) was modified with the as-prepared catalysts and used as working electrodes, which was performed as following: 8 mg Pt/Ni/NCNTs was first added to a mixture of 8 mL anhydrous ethanol and 10 μ L Nafion solution, and then sonicated for 10 min to obtain a well-mixed suspension. GCE was polished with Al₂O₃ powder and rinsed several times with deionized water, then dried after ultra-sonication



Scheme 1 Schematic illustration of the formation process of Pt/Ni/NCNTs

with deionized water for 5 min. Ten microliter catalyst suspension was dropped onto the surface of GCE and dried at 60 °C for 30 min to obtain a Pt/Ni/NCNTs/GCE working electrode. Counter and reference electrodes were platinum sheets and Ag/AgCl, respectively. CVs were performed at a fixed potential range with scan rates ranging from 10 to 150 mV/s or with constant scan rate (50 mV/s) at various nitrite concentrations. I–T curves were carried out by continuously adding a certain amount of nitrite to the electrolyte solution with the applied potential of 1.0 V, during which the N_2 flow was continuously inflated to mitigate the effects of the electrolyte diffusion. Zahner Zennium electrochemical workstations were used to carry out electrochemical impedance spectroscopy (EIS) measurement.

X-ray photoelectron spectroscopy (XPS), X-ray diffraction (XRD), and scanning electron microscopy (SEM) were employed to investigate the constituent and structures of the electrode materials. Detailed information was listed in the Supplementary Materials (Sect. 1).

Results and discussion

The fabrication procedure for the Pt/Ni/NCNTs is schematically illustrated in Scheme 1. First, polyhedral Ni-MOF can be fabricated through the coordination of nickel ions with 2-methylimidazole. Then, the Ni-MOF, as self-sacrificing template can be transformed into Ni/NCNTs during the reduction and carbonation process at 900 °C in N_2 atmosphere. During the thermal annealing process, the Ni nanoparticles in situ reduced from Ni-MOF acted as catalysts, the organic ligands as carbon and nitrogen source to facilitate the formation of NCNTs. Finally, the Pt/Ni/NCNT was obtained by microwave-assisted ethylene glycol reduction method. The morphology of Pt/Ni/NCNTs and Ni/NCNTs was characterized with SEM (Fig. 1). Both samples present a typical tubular frame with very large aspect ratio. The surface of Ni/NCNTs is relatively smooth (Fig. 1a and b), indicating the relatively tight and firm combination of Ni and NCNTs through this in situ growth process. After deposition of Pt, the surface of Pt/Ni/NCNTs turned relatively rough (Fig. 1c and d). Pt nanoparticles can be clearly found on the

tube surface. Figure 2 displays the EDS mapping of Ni, Pt, C, and N for Pt/Ni/NCNTs. The elements of Ni, Pt, C, and N homogeneously distributed on the whole nano-tubular structures, indicating the successful formation of Pt/Ni/NCNTs.

Figure 3 shows the XRD patterns of Ni/NCNTs and Pt/Ni/NCNTs, both of which present typical diffraction peaks of metallic Ni with 2θ at 44.3°, 51.6°, and 76.2° corresponding to its (111), (200), and (220) crystal planes (JCPDS no. 04–0850). By comparison, it can be investigated that in addition to the signal of Ni, there are obvious diffraction peaks of cubic crystalline Pt (JCPDS no. 04–0802) on the Pt/Ni/NCNTs pattern. The diffraction peaks of (1 1 1) (39.8°), (2 0 0) (46.2°), and (2 2 0) (67.5°) facets for Pt appear distinctly broadened and weak comparing with Ni, implying low content and smaller diameter of Pt on NCNTs. Moreover, a very weak peak is observed on both XRD patterns at 2θ of 26.2°, which belongs to the (002) crystal plane of graphitic carbon (JCPDS no. 41–1487), suggesting the formation of NCNTs. The results prove the successful integration of Pt, Ni, and NCNTs.

Pt/Ni/NCNTs were further characterized by XPS to analyze their surface chemical composition and valence. The XPS survey spectrum (Fig. S1) verified that Pt/Ni/NCNTs mainly contain platinum, nickel, carbon, and nitrogen elements. Deconvoluted Pt 4f spectrum (Fig. 4a) displays two main peaks at 71.2 and 74.5 eV corresponding to the characteristic binding energy of metallic Pt 4f_{7/2} and Pt 4f_{5/2}, suggesting that the dominant valence state of Pt in Pt/Ni/NCNTs is Pt⁰. Moreover, the other two weak peaks (72.2 and 75.6 eV) belonging to Pt²⁺ may be caused by a slight oxidation of the Pt surface [20, 21]. Ni 2p spectrum is presented in Fig. 4b, which shows two pairs of Ni 2p with satellite peaks at 860.9 and 879.1 eV. The peaks at 853.4 and 855.5 eV belong to the Ni⁰ 2p_{3/2} and Ni²⁺ 2p_{3/2}, respectively. Another two peaks at 871.2 and 873.1 eV can be attributed to Ni⁰ 2p_{1/2} and Ni²⁺ 2p_{1/2} states, respectively [22, 23]. N 1s spectrum (Fig. 4c) proves the presence of three types of nitrogen species: pyridinic N (398.8 eV), pyrrolic N (399.8 eV), and graphitic N (400.9 eV) [22, 24]. Figure 4d shows the C 1s spectrum, which is resolved into three peaks belonging to functional bonds of C–C (284.5 eV), C–N (286.0 eV), and C–O (288.3 eV) [18, 25].

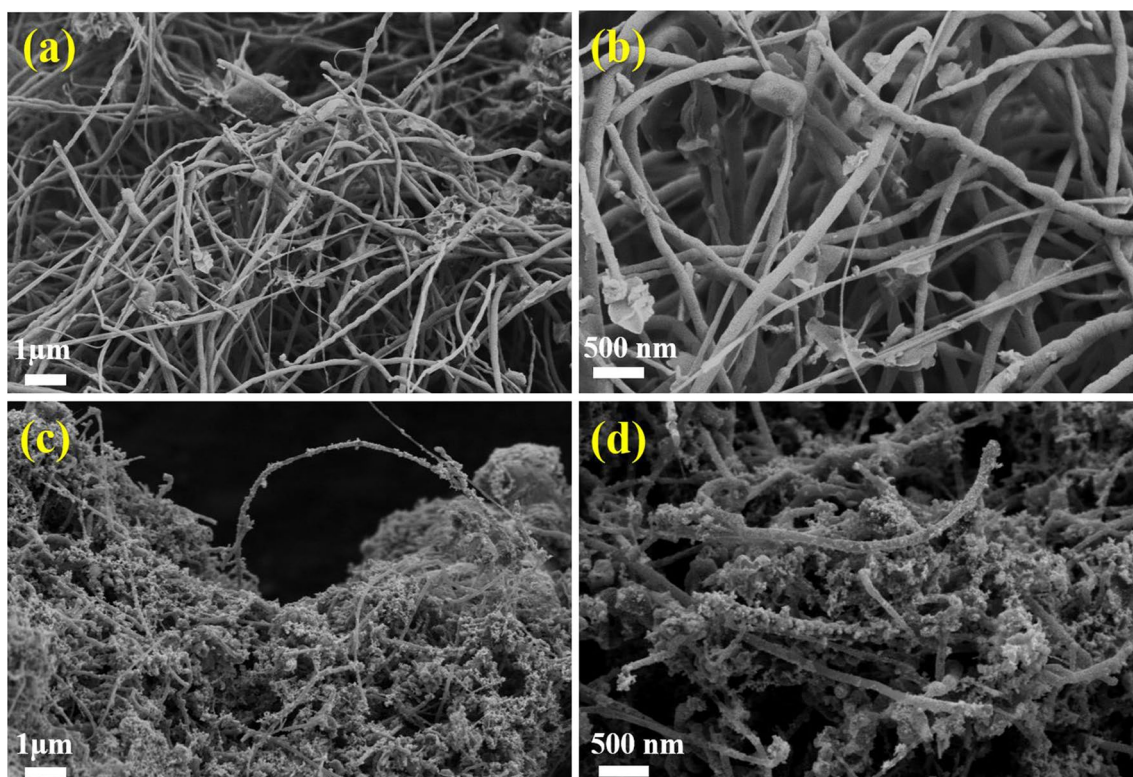


Fig. 1 SEM images of Ni/NCNTs (a, b) and Pt/Ni/NCNTs (c, d)

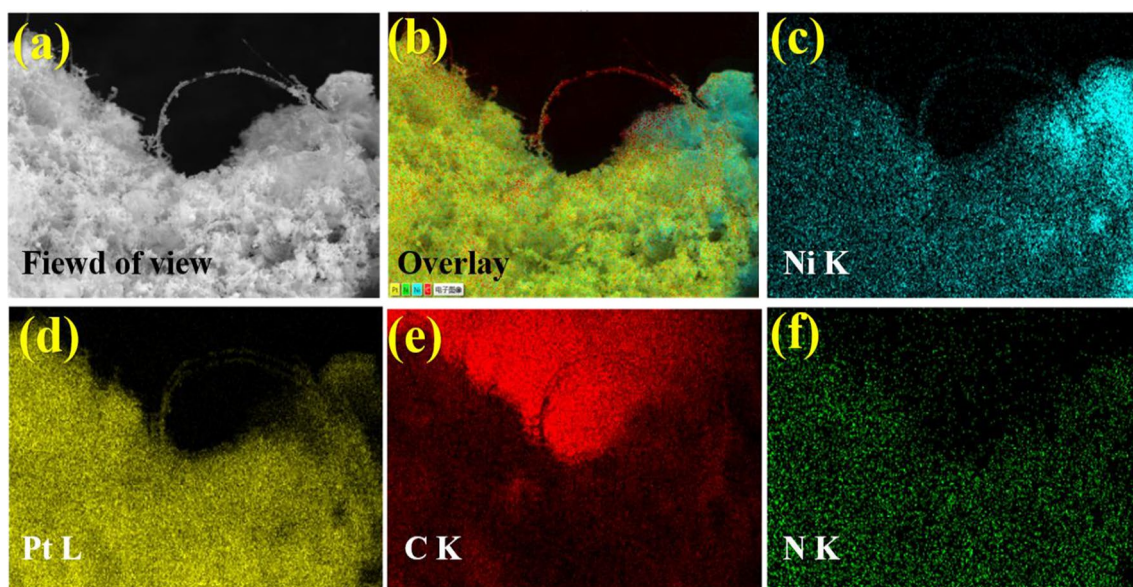


Fig. 2 EDS mapping of the Ni, Pt, C, and N for Pt/Ni/NCNTs (signals were obtained from K line of Ni, C, and N elements and L line of Pt element)

The electrochemical properties of Pt/Ni/NCNTs and Ni/NCNTs were examined through CVs (Fig. 5a) and DPVs (Fig. 5b) in 0.1 M PBS in absence and presence of 1 mM

nitrite. A distinct anodic peak for nitrite oxidation can be observed on CVs curve of Pt/Ni/NCNTs at about 0.85 V, while Ni/NCNTs only appear a broaden peak at 1.0 V,

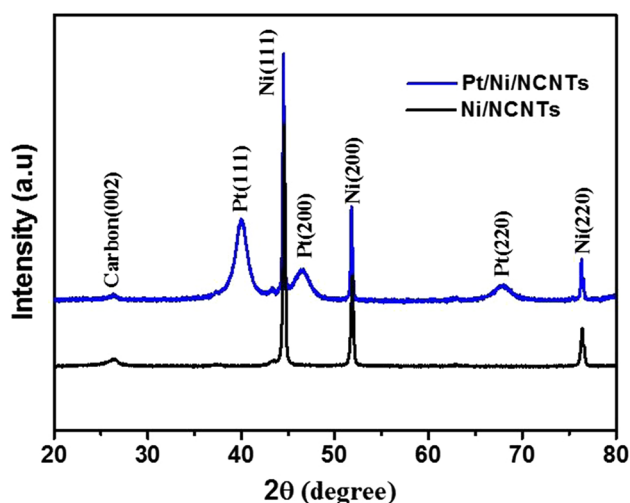


Fig. 3 XRD of Pt/Ni/NCNTs and Ni/NCNTs

suggesting better catalytic activity of Pt/Ni/NCNTs. The difference of anodic peak current can be more clearly observed on the DPVs with the net current increase of Pt/Ni/NCNTs (25.02 μA) more than four times higher than that of Ni/NCNTs (7.83 μA). In addition, the anodic peak potential of Pt/Ni/NCNTs is significantly lower than Ni/NCNTs on both the CVs and DPVs plots. More importantly, no oxidation peaks are observed on both CVs and DPVs in absence of nitrite, suggesting that the current response on both Pt/Ni/NCNTs and Ni/NCNTs electrodes is mainly due to the nitrite oxidation rather than the electrode material. The CVs and DPVs results suggest that the deposition of Pt on Ni/NCNTs may both increase their catalytic activities and lower the operating voltages.

The interfacial properties of Ni/NCNTs and Pt/Ni/NCNTs were evaluated through EIS to identify the difference of their activities for nitrite oxidation. The EIS curves measured in 5 mM $[\text{Fe}(\text{CN})_6]^{3-}/[\text{Fe}(\text{CN})_6]^{4-}$ solution with 0.1 M KCl as supporting electrolyte are presented in Fig. 5. The Nyquist

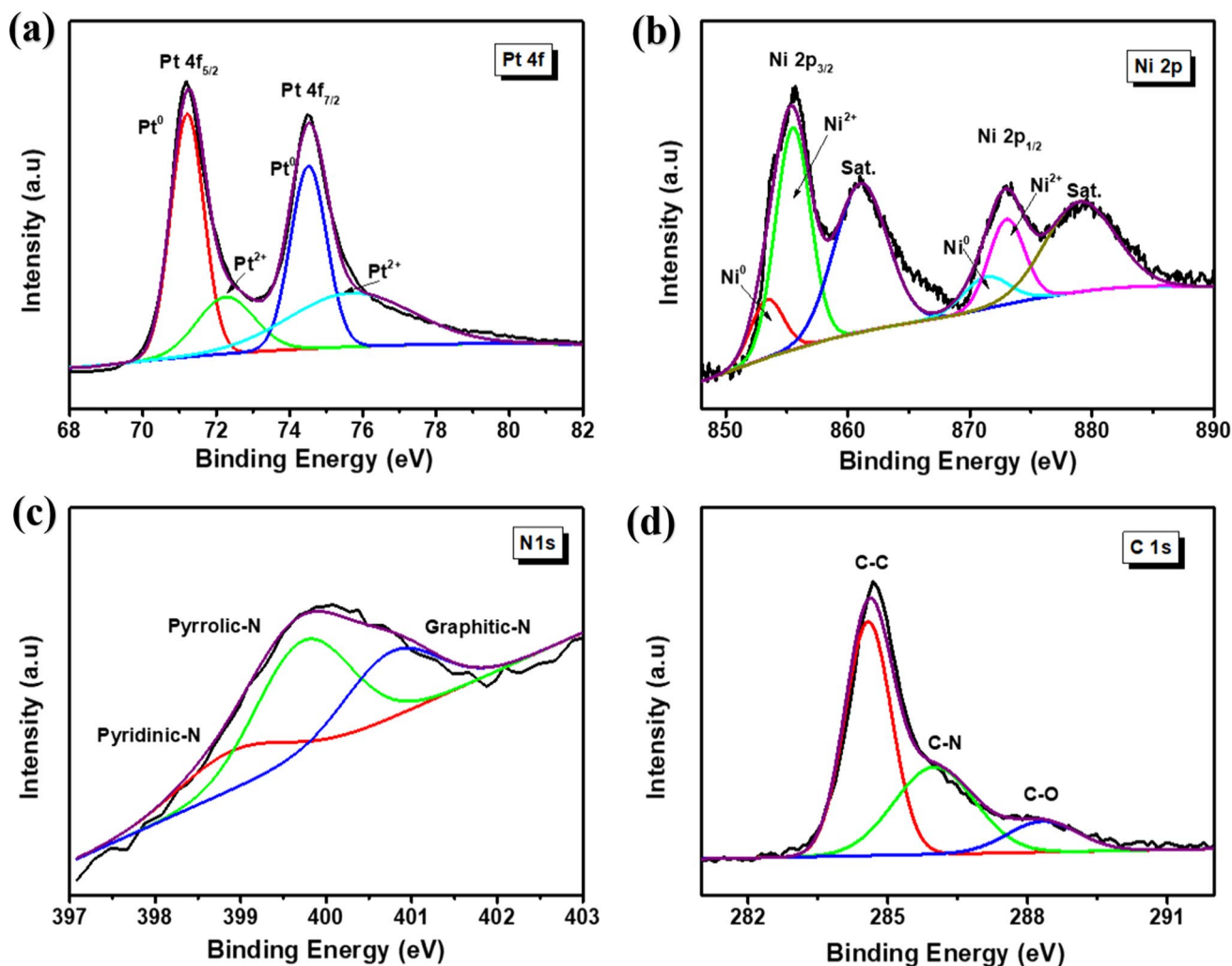


Fig. 4 XPS spectrum of Pt 4f (a), Ni 2p (b), N 1s (c), and C 1s (d) in Pt/Ni/NCNTs

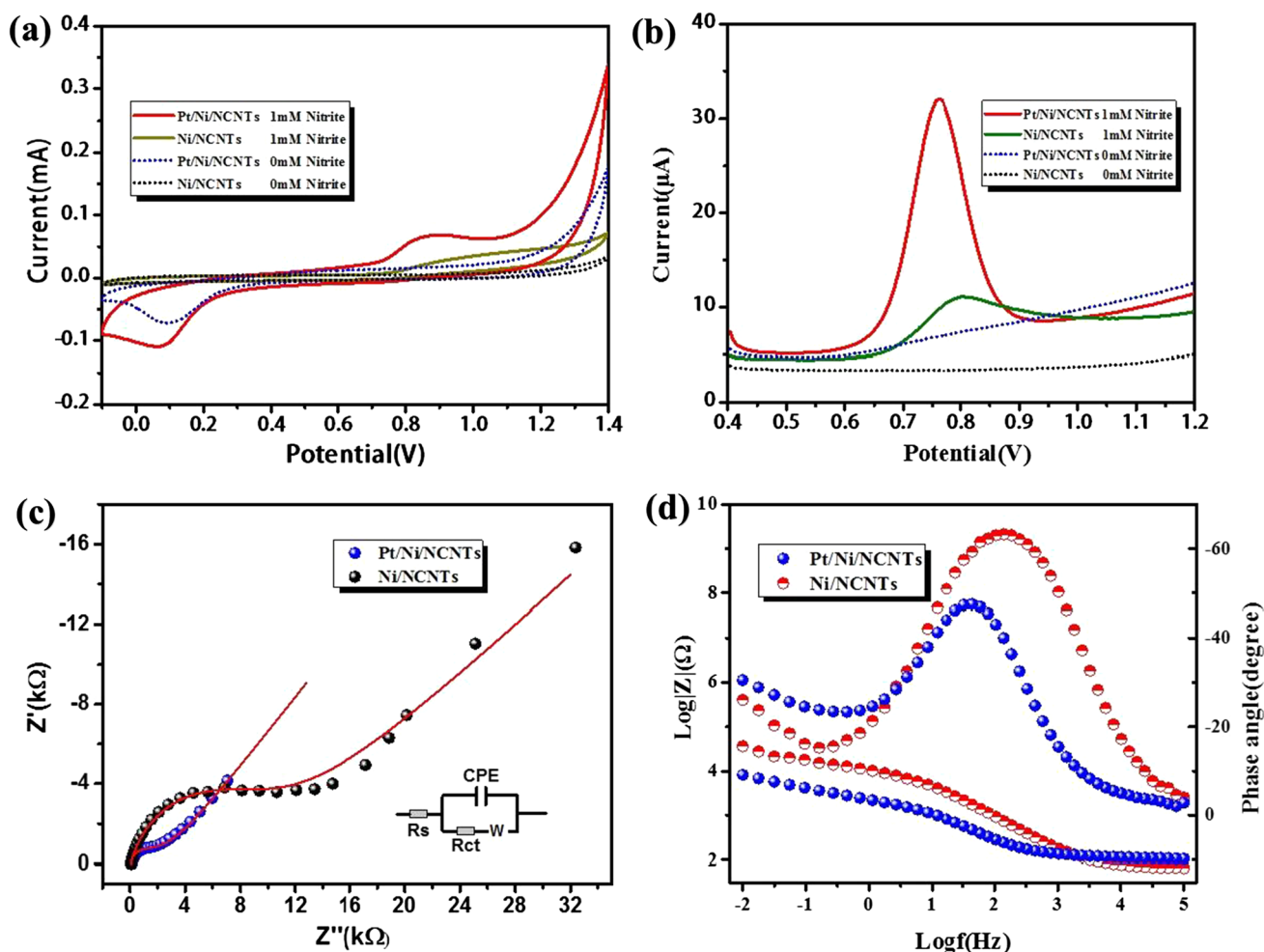


Fig. 5 CVs (a) and DPVs (b) for Pt/Ni/NCNTs and Ni/NCNTs with (solid curves) and without (dotted curves) nitrite; EIS Nyquist plots (c) and Bode plots (d) of Pt/Ni/NCNTs and Ni/NCNTs recorded in the electrolyte of 0.1 M KCl containing 1 mM $[\text{Fe}(\text{CN})_6]^{3-/4-}$

plots (Fig. 5c) display a typical semicircle in the high frequency region and linear part at lower-frequency region, which correspond to electron transfer (R_{ct}) and the diffusion-limited process, respectively [26, 27]. The semicircle of Pt/Ni/NCNTs is much smaller than Ni/NCNTs indicating the fast charge transfer efficiency of Pt/Ni/NCNTs. The equivalent circuit is inserted in Fig. 5c and corresponding parameters are listed in Table S1. The R_{ct} of Pt/Ni/NCNTs ($1.05 \times 10^2 \Omega$) is much lower than Ni/NCNTs ($3.15 \times 10^3 \Omega$), indicating the deposition of Pt nanoparticles on Ni/NCNTs can evidently reduce charge transfer resistance and improve the heterogeneous electron transfer process, which is beneficial for nitrite oxidation. Bode plots in Fig. 5d display one typical time constant which is consistent with the fitting results of Nyquist plots. Bode modulus plots also proved the lower $|Z|$ of Pt/Ni/NCNTs. Lower phase angle of Pt/Ni/NCNTs further implies that the charge transfer reaction is facilitated on Pt/Ni/NCNTs as the phase angle of 90° represents an ideal capacitor [26]. The results suggest that the

improved nitrogen oxidation on Pt/Ni/NCNTs may benefit from the increased charge transfer efficiency originating from the deposition of Pt.

The electrochemical sensing properties of Pt/Ni/NCNTs were further evaluated by CVs (Fig. 6a) and DPVs (Fig. 6b) with different nitrite in 0.1 M PBS. As the concentration increased, both oxidation currents of nitrite in CVs and DPVs curves increase synchronously. A good linear relationship can be obtained by plotting the normalization of current and nitrite concentration. The linear regression equation of CVs results is $I_p (\mu\text{A}) = 0.0309C (\mu\text{M}) - 36.528$ ($R^2 = 0.996$) (Insert in Fig. 6a). Plots of DPVs current (Insert in Fig. 6b) present the regression equation of $I_p (\mu\text{A}) = 0.0336C (\mu\text{M}) + 5.054$ ($R^2 = 0.999$). The results suggest that Pt/Ni/NCNTs electrode is sensitive to the nitrite concentration and can be used as a promising electrode material for nitrite sensing application.

The effect of scan rate (ν) on CVs of Pt/Ni/NCNTs was performed to further evaluate the kinetics of nitrite

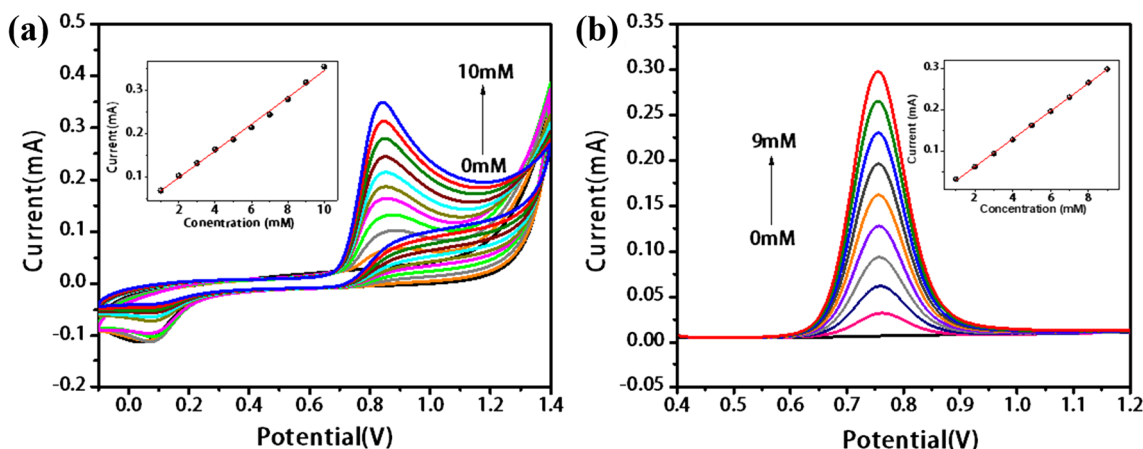


Fig. 6 CVs (a) and DPVs (b) of Pt/Ni/NCNTs with various nitrite (Inserts are their plots of concentration vs. currents)

oxidation. Figure 7 presents the CVs of Pt/Ni/NCNTs depending on various ν in 0.1 M PBS containing nitrite. Anodic peak current (I_{pa}) can be clearly found increasing gradually with ν varying from 10 to 150 mV/s (Fig. 7a). The linear relationship of I_{pa} vs. $\nu^{1/2}$ (Fig. S2a) can be obtained on the Pt/Ni/NCNTs electrodes. Accordingly, the linear regression equation for $\log \nu$ vs. $\log I_{pa}$ (insert in Fig. 7a) is given by $\log I_{pa} = 0.51668 \log \nu + 1.04098$ ($R^2 = 0.995$). It is well known that the theoretical value of the slope for diffusion control process is 0.5. If the slope is close to 1, the electrochemical reaction occurs via an adsorption-controlled process [12, 28]. The slope value of 0.51668 is close to the theoretical value of 0.5 indicating the diffusion control process for nitrite oxidation on the Pt/Ni/NCNTs electrodes. Moreover, the anodic peak potential (E_{pa}) in CVs has a slight shift with ν increasing, which may indicate that the oxidation of nitrite is an irreversible process. Fig. S2b displays the linear relationship of E_{pa} vs. $\ln \nu$ with the equation

of E_{pa} (V) = $0.04397 \ln \nu$ ($\ln V s^{-1}$) + 0.67499 ($R^2 = 0.994$). According to the Laviron's equation, α and the number of electrons (n) were calculated to be 0.56 and 1.04 (detailed calculation is listed in supporting materials "Experimental section"), indicating a fast electron transfer process with one electron involved in the oxidation of nitrite [13, 25]. Figure 7b gives the plot of $\log I$ vs. E (insert on Fig. 7b) based on the data from rising part of E-I curve measured with scan rate of 1 mV/s. The linearity can be described by the following regression approximation: $\log I = 6.48244 \eta - 10.23735$. The slope value of 6.48244 in the equation is equal to Tafel slope of $n(1-\alpha)F/2.3RT$, 29. According to the estimated α (0.56) above, n was calculated to be 0.87, which is also close to 1. Therefore, the rate-determining step during nitrite oxidation on Pt/Ni/NCNTs electrodes may undergo a one electron transfer process. The mechanism of nitrite oxidation can be described as followings according to previous reports [30, 31].

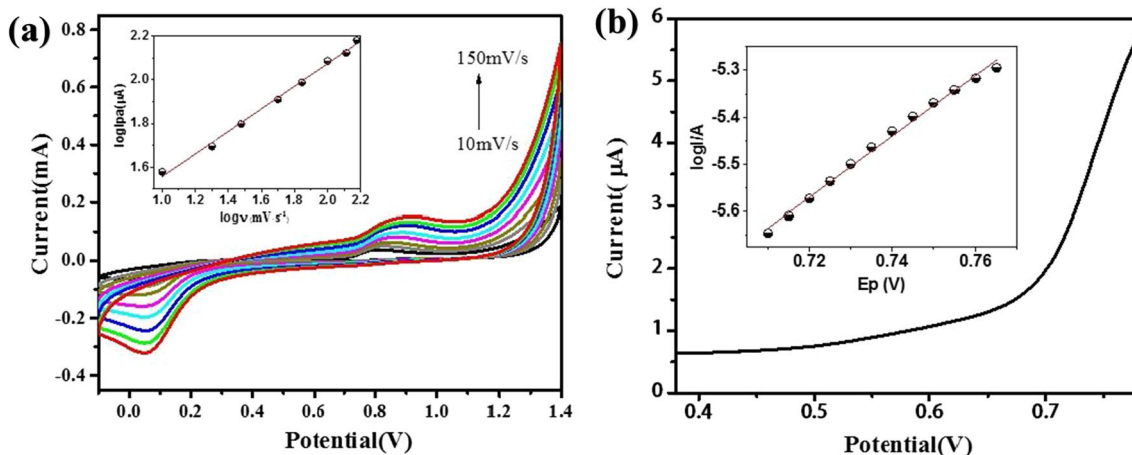
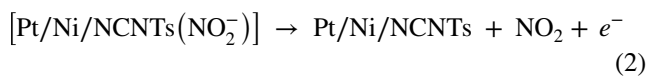
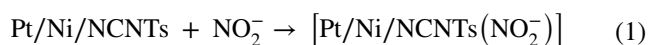


Fig. 7 a CVs for Pt/Ni/NCNTs with various scan rates (10 mV/s-150 mV/s) in PBS containing 1 mM nitrite (Inserts: Plots of $\log \nu$ vs. $\log I_{pa}$), b Rising part of CVs recorded with scan rate of 1 mV/s (Inserts: Tafel plots of $\log I$ vs. E_{pa})



Nitrite can first adsorb on Pt/Ni/NCNTs to form the complex of $[\text{Pt/Ni/NCNTs}(\text{NO}_2^-)]$. Then, one electron was lost on $[\text{Pt/Ni/NCNTs}(\text{NO}_2^-)]$ to produce NO_2 . Finally, NO_2 will transfer to NO_2^- and NO_3^- through a disproportionation reaction.

The applied potential has been optimized as it can distinctly affect the current response of nitrite oxidation. Various applied potentials were explored to record amperometric response of Pt/Ni/NCNTs (Fig. S3), which shows an increase

of current response with the applied potentials varying from 0.7 to 1.1 V. Considering that more noise signals may be introduced at the higher applied potentials, 1.0 V was used as the optimal potential. The nitrite sensing performance of Pt/Ni/NCNTs was further evaluated by measuring the amperometric response at the optimal potential with successive addition of nitrite (Fig. 8a). The current response of both Pt/Ni/NCNTs and Ni/NCNTs presents distinct increase step by step with the addition of nitrite. Moreover, Pt/Ni/NCNTs demonstrate a much stronger current response with the linear plot of current vs. nitrite concentration presented in Fig. 8b. The fitting results displayed that the Pt/Ni/NCNTs sensors presented excellent sensing performance for nitrite detection with much higher detection ranges of 0.5–40 mM and 40–110 mM. The sensitivity in the range of 0.5–40 mM is $276.92 \mu\text{A mM}^{-1} \text{cm}^{-2}$ with the detection limit of 0.17 μM . The sensitivity in another range (40–110 mM)

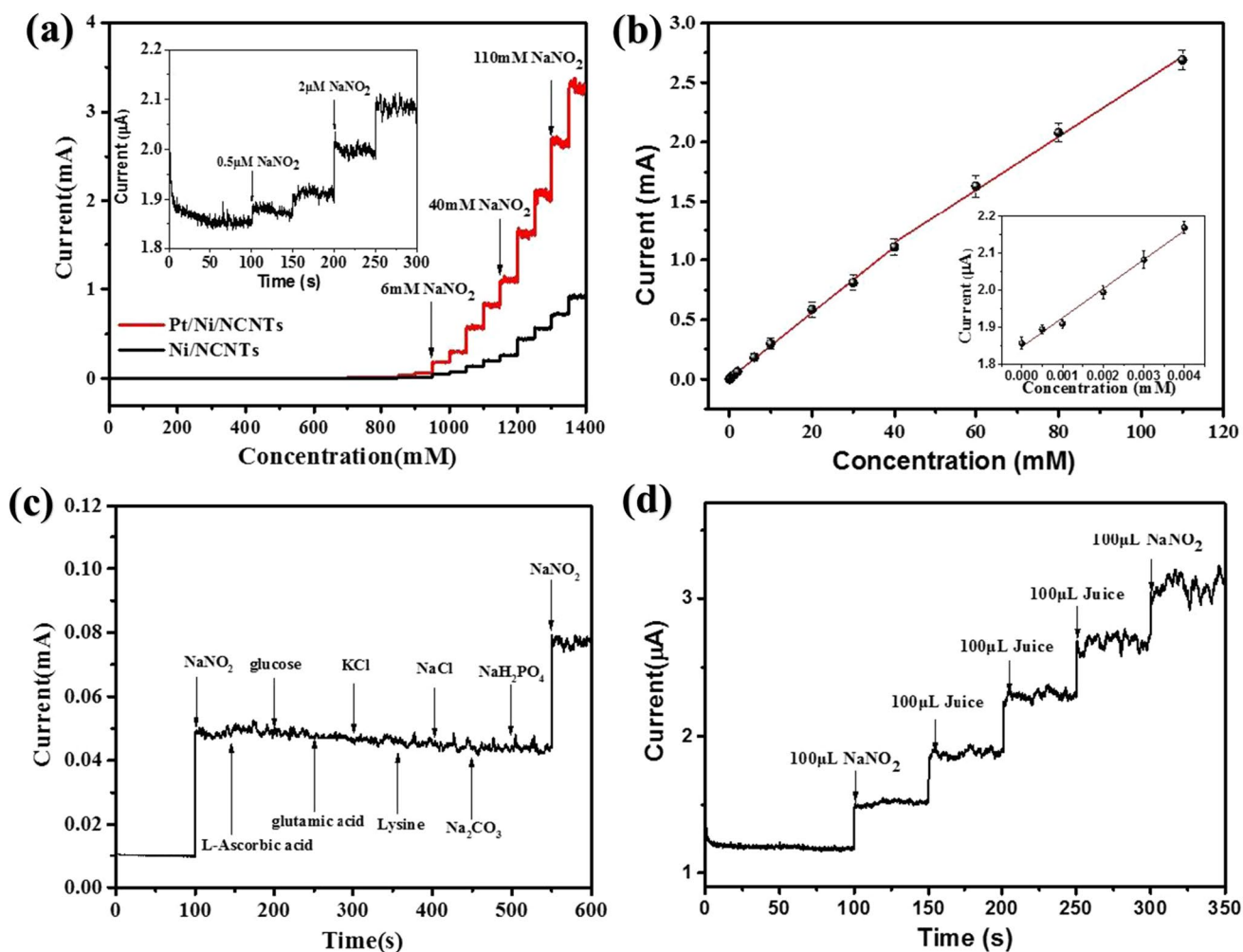


Fig. 8 a Amperometric current response to continuous injection of nitrites at potential of 1.0 V (Inserts: amplified amperometric (I-T) curves in low nitrite concentration), b Plots of current vs. nitrite con-

centration (Insert: the plots in the range of 0–4 μM), c Interference test for Pt/Ni/NCNTs to various interferences, d Typical amperometric (I-T) curves of Pt/Ni/NCNTs for peach juice analysis

Table 1 Comparison of Pt/Ni/NCNTs with other nitrite sensors

Sensors	Linear range (μM)	Detection limit (μM)	Sensitivity ($\mu\text{A mM}^{-1} \text{ cm}^{-2}$)	References
Pt/Ni/NCNTs	0.5–40,000 40,000–110,000	0.17	276.92 224.39	This work
$\alpha\text{-Fe}_2\text{O}_3/\text{CNTs}$	0.5–4000	0.15	334	[14]
Ag/HNTs/MoS ₂ -CPE	2–425	0.7	89.9	[32]
Nickel oxide/graphene	5–8000	0.98	0.0184	[12]
Pt/Ni(OH) ₂ /MWCNTs	0.4–5670	0.13	145	[33]
Au NPs/MoS ₂	5–277,800	1.7	117.0	[34]
Ni/MoS ₂ /GCE	20–1000	2.74	15.09	[35]

is $224.39 \mu\text{A mM}^{-1} \text{ cm}^{-2}$. The results suggest that Pt/Ni/NCNTs present much wider detection range and excellent sensitivity for nitrite sensing compared with other previous nitrite sensors (Table 1), indicating the sensors may be applied in a wide range of conditions which is very helpful for the real-time detection of nitrite.

The selectivity of Pt/Ni/NCNTs was also studied by measuring the I–T curves with contentiously adding different interfering substances to 0.1 M PBS. With the applied potential of 1.0 V, 0.2 mM NaNO₂, 2 mM L-ascorbic acid, 2 mM glucose, 2 mM glutamic acid, 2 mM KCl, 2 mM Lysine, 2 mM NaCl, 2 mM Na₂CO₃, 2 mM NaH₂PO₄, and 0.2 mM NaNO₂ were added continuously to 0.1 M PBS, and the I–T curves are showed in Fig. 8c. It can be observed that distinct current response was obtained with the addition of nitrite. On the contrary, interference species display negligible current signals on the I–T curves. The results indicate that Pt/Ni/NCNTs have good selectivity for nitrite detection. Nitrite levels were also analyzed with real samples (spiked milk and peach juice) to assess the practical applicability of Pt/Ni/NCNTs. The nitrite level was performed with standard addition method through recording the amperometric (I–T) response. The typical amperometric (I–T) curves with injecting 100 μL NaNO₂, 100 μL peach juice are presented in Fig. 8d and the corresponding curves of milk are showed in Fig. S4. The satisfied recoveries fall within the range of 95.8–104.5%, suggesting Pt/Ni/NCNTs are feasible for real sample applications.

Conclusions

Newly developed nitrite sensors using Pt/Ni/NCNTs as electrode materials were successfully obtained through depositing Pt on self-catalytically grown Ni-/N-doped carbon nanotubes. According to CVs, DPVs, EIS, and I–T measurement, Pt/Ni/NCNTs displayed superior electrochemical performance for nitrite oxidation due to the synergy of Pt and Ni/NCNTs. The Pt/Ni/NCNTs sensors present excellent nitrite sensing properties including high sensitivity

of $276.92 \mu\text{A mM}^{-1} \text{ cm}^{-2}$ in the range of 0.5–40 mM and $224.39 \mu\text{A mM}^{-1} \text{ cm}^{-2}$ in the range of 40–110 mM and low detection limit of 0.17 μM . High selectivity was also obtained on Pt/Ni/NCNTs in presence of interferents. In addition, satisfactory results were also achieved for nitrite detection in real samples (milk and peach juice) analysis. The results may have some inspiration for the development of new efficient electrochemical sensors based on Pt relative and MOF-derived materials.

Supplementary Information The online version contains supplementary material available at <https://doi.org/10.1007/s44211-023-00336-2>.

Acknowledgements This work was financially supported by Zhejiang natural science foundation (No. Y19E060021).

Data availability The datasets generated during and/analyzed during the current study are available from the corresponding author on reasonable request.

Declarations

Conflict of interest The authors have no competing interests to declare relevant to this article's content.

References

- V. Mariyappan, S.-M. Chen, K. Murugan, A. Jeevika, T. Jeyapragasam, R. Ramachandran, *Colloids Surf. A* **637**, 128271 (2022). <https://doi.org/10.1016/j.colsurfa.2022.128271>
- A.R. Marlinda, M.N. Anamt, N. Yusoff, S. Sagadevan, Y.A. Wahab, M.R. Johan, *Trends Environ. Anal. Chem.* **34**, e00162 (2022). <https://doi.org/10.1016/j.teac.2022.e00162>
- Z. Yang, Y. Zhong, X. Zhou, W. Zhang, Y. Yin, W. Fang et al., *J. Food Measur. Charact.* **16**(2), 1572–1582 (2022). <https://doi.org/10.1007/s11694-021-01270-5>
- J. Wu, X. Wang, Y. Lin, Y. Zheng, J.-M. Lin, *Talanta* **154**, 73–79 (2016). <https://doi.org/10.1016/j.talanta.2016.03.062>
- Z. Ma, J. Li, X. Hu, Z. Cai, X. Dou, *Adv. Sci.* **7**(24), 2002991 (2020). <https://doi.org/10.1002/adv.202002991>
- P. Singh, M.K. Singh, Y.R. Beg, G.R. Nishad, *Talanta* **191**, 364–381 (2019). <https://doi.org/10.1016/j.talanta.2018.08.028>
- H.S. Lim, S.J. Lee, E. Choi, S.B. Lee, H.S. Nam, J.K. Lee, *Food Chem.* **382**, 132280 (2022). <https://doi.org/10.1016/j.foodchem.2022.132280>

8. M. Shivakumar, S. Manjunatha, K.N. Nithyayini, M.S. Dharmaprakash, K.L. Nagashree, *J. Elect. Chem.* **882**, 115016 (2021). <https://doi.org/10.1016/j.jelechem.2021.115016>
9. T. Zhe, M. Li, F. Li, R. Li, F. Bai, T. Bu et al., *Food Chem.* **367**, 130666 (2022). <https://doi.org/10.1016/j.foodchem.2021.130666>
10. Y. Ma, Y. Wang, D. Xie, Y. Gu, H. Zhang, G. Wang et al., *ACS Appl. Mater. Interfaces.* **10**(7), 6541–6551 (2018). <https://doi.org/10.1021/acsami.7b16536>
11. S. Lu, M. Hummel, X. Wang, W. He, R. Pathak, X. Dong et al., *J. Elect. Soc.* **167**(14), 146517 (2020). <https://doi.org/10.1149/1945-7111/abc99d>
12. W. Yi, Z. Li, W. Dong, C. Han, Y. Guo, M. Liu et al., *ACS Appl. Nano Mater.* **5**(1), 216–226 (2022). <https://doi.org/10.1021/acsnm.1c02690>
13. F. Mollarasouli, M.R. Majidi, K. Asadpour-Zeynali, *Electrochim. Acta* **291**, 132–141 (2018). <https://doi.org/10.1016/j.electacta.2018.08.132>
14. K. Wang, C. Wu, F. Wang, C. Liu, C. Yu, G. Jiang, *Electrochim. Acta* **285**, 128–138 (2018). <https://doi.org/10.1016/j.electacta.2018.07.228>
15. Z. Zhao, J. Zhang, W. Wang, Y. Sun, P. Li, J. Hu et al., *Appl. Surf. Sci.* **485**, 274–282 (2019). <https://doi.org/10.1016/j.apsusc.2019.04.202>
16. L. Wu, X. Zhang, M. Wang, L. He, Z. Zhang, *Measurement* **128**, 189–196 (2018). <https://doi.org/10.1016/j.measurement.2018.06.041>
17. Q. Lu, J. Yu, X. Zou, K. Liao, P. Tan, W. Zhou et al., *Adv. Func. Mater.* **29**(38), 1904481 (2019). <https://doi.org/10.1002/adfm.201904481>
18. D. Bin, B. Yang, C. Li, Y. Liu, X. Zhang, Y. Wang et al., *ACS Appl. Mater. Interfaces.* **10**(31), 26178–26187 (2018). <https://doi.org/10.1021/acsami.8b04940>
19. Y. Lu, H. Zhang, E.H. Ang, Z. Nie, H. Liu, Y. Du et al., *Mater. Today Phys* **16**, 100303 (2021). <https://doi.org/10.1016/j.mtphys.2020.100303>
20. T.P. Wang, P.Y. Tsou, C.L. Lee, *Int. J. Energy Res.* **46**(6), 8491–8502 (2022). <https://doi.org/10.1002/er.7710>
21. X. Xu, Z. Ma, D. Li, Z. Su, X. Dong, H. Huang et al., *ACS Appl. Nano Mater.* **5**(4), 4983–4990 (2022). <https://doi.org/10.1021/acsnm.1c04575>
22. T. Dong, X. Zhang, Y. Cao, H.-S. Chen, P. Yang, *Inorg. Chem. Front.* **6**(4), 1073–1080 (2019). <https://doi.org/10.1039/c8qi01335g>
23. Z. Wang, L. Cheng, R. Zhang, W. Lv, W. Wang, *J. Alloys Comp.* **857**, 158249 (2021). <https://doi.org/10.1016/j.jallcom.2020.158249>
24. M. Yao, B. Wang, N. Wang, S. Komarneni, Y. Chen, J. Wang et al., *ACS Sust. Chem. Eng.* **8**(13), 5287–5295 (2020). <https://doi.org/10.1021/acssuschemeng.0c00268>
25. D. Zhu, Q. Zhen, J. Xin, H. Ma, L. Tan, H. Pang et al., *Sens. Act. B* **321**, 128541 (2020). <https://doi.org/10.1016/j.snb.2020.128541>
26. T. Ghosh, P. Sarkar, A.P. Turner, *Bioelectrochemistry* **102**, 1–9 (2015). <https://doi.org/10.1016/j.bioelechem.2014.11.001>
27. M.R. Hasan, T. Islam, M.M. Hasan, A.-N. Chowdhury, A.J.S. Ahammad, A.H. Reaz et al., *J. Phys. Chem. Solids* **165**, 110659 (2022). <https://doi.org/10.1016/j.jpcs.2022.110659>
28. M. Sookhajian, M.A. Mat Teridi, G.B. Tong, P.M. Woi, M. Khalil, Y. Alias, *ACS Appl. Nano Mater.* **4**(11), 12737–12744 (2021). <https://doi.org/10.1021/acsnm.1c03351>
29. M. Faisal, M.A. Rashed, M.M. Abdullah, F.A. Harraz, M. Jalalah, M.S. Al-Assiri, *J. Elect. Chem.* **879**, 114805 (2020). <https://doi.org/10.1016/j.jelechem.2020.114805>
30. B. Dou, J. Yan, Q. Chen, X. Han, Q. Feng, X. Miao et al., *Sens. Actuat. B* **328**, 129082 (2021). <https://doi.org/10.1016/j.snb.2020.129082>
31. E. Saeb, K. Asadpour-Zeynali, *Electrochim. Acta* **417**, 140278 (2022). <https://doi.org/10.1016/j.electacta.2022.140278>
32. M. Ghanei-Motlagh, M.A. Taher, *Biosens. Bioelectron.* **109**, 279–285 (2018). <https://doi.org/10.1016/j.bios.2018.02.057>
33. Q. Sheng, D. Liu, J. Zheng, *J. Electroanal. Chem.* **796**, 9–16 (2017). <https://doi.org/10.1016/j.jelechem.2017.04.050>
34. S. Zhang, Y. Tang, Y. Chen, J. Zheng, *J. Electroanal. Chem.* **839**, 195–201 (2019). <https://doi.org/10.1016/j.jelechem.2019.03.036>
35. Y. Yang, J. Zhang, Y.W. Li, Q. Shan, W. Wu, *Colloids Surf A* **625**, 126865 (2021). <https://doi.org/10.1016/j.colsurfa.2021.126865>

Springer Nature or its licensor (e.g. a society or other partner) holds exclusive rights to this article under a publishing agreement with the author(s) or other rightsholder(s); author self-archiving of the accepted manuscript version of this article is solely governed by the terms of such publishing agreement and applicable law.